ADVANCED MATERIALS
www.advmat.de

High-Mobility Transistors Based on Large-Area and Highly Crystalline CVD-Grown $MoSe_2$ Films on Insulating Substrates

Jong-Soo Rhyee, Junyeon Kwon, Piyush Dak, Jin Hee Kim, Seung Min Kim, Jozeph Park, Young Ki Hong, Won Geun Song, Inturu Omkaram, Muhammad A. Alam, and Sunkook Kim**

Recent advances in high-performance mechanically flexible/stretchable electronics are anticipated to promote the advent of new electronic applications such as flexible organic light-emitting diode (OLED) displays[1] or human-centric soft electronics including epidermal devices[2,3] and biomedical systems.[4–7] Increasing demands for high-performance active devices for such applications also necessitate their mechanical and electrical reliability in various bending/flexible environments. Thin film transistors (TFTs) based on amorphous and polycrystalline silicon are currently the major semiconductor materials used to fabricate active-matrix OLED (AMOLED) or liquid crystal display (LCD) backplanes, but their relatively low field effect mobility and mechanically fragile nature limit their use in flexible electronics. In this regard, layered semiconductors based on transition metal dichalcogenides (TMDCs): MX_2 = Mo, W; X = S, Se, Te exhibit desirable characteristics including high mobility (>100 $cm^2 V^{-1} s^{-1}$), wide band gap (E_g > 1 eV), and mechanical flexibility, which make them promising as active elements in future high-performance flexible/stretchable integrated circuitry.[8–10] Earlier investigations involved the study of the exotic electronic and mechanical properties of TMDCs by preparing atomically thin flakes using scotch tape assisted exfoliation or electrochemical intercalation from pristine bulk crystals.[11–13] However, several key challenges lie ahead before such TMDC flakes can be integrated into complex circuits, because the above methods do not provide large-area coverage and systematic control of the film thickness.

Prof. J.-S. Rhyee, J. H. Kim
Department of Applied Physics
Kyung Hee University
Yongin 17104, Korea
J. Kwon, J. Park, Y. K. Hong, W. G. Song, I. Omkaram, Prof. S. Kim
Multi-Functional Nano/Bio Electronics Laboratory
Kyung Hee University
Gyeonggi 17104, Korea
E-mail: kimskcnt@gmail.com
P. Dak, Prof. M. A. Alam
School of Electrical and Computer Engineering
Purdue University
West Lafayette, IN 47907, USA
E-mail: alam@purdue.edu
Dr. S. M. Kim
Carbon Convergence Materials Research Center
Korea Institute of Science and Technology
Wanju-gun 565-905, Republic of Korea

DOI: 10.1002/adma.201504789

Reproducible large-area production of 2D layered semiconductors is thus essential in order to implement their intriguing properties into large-area integrated circuitry. Several studies on the thermal chemical vapor deposition (CVD) of large-area monolayer or multilayer MoS_2 have been reported recently, including direct sulfurization of MoO_3 or pre-deposited Mo metal films,[14,15] gas-phase reaction of MoO_3 and S powders,[16–18] and two-step thermolysis of solution-type[19] ammonium thiomolybdates $(NH_4)_2MoS_4$ in an inert gas and H_2, which allow the synthesis of high-quality monolayer MoS_2 over wafer scale large area. However, large-scale synthetic MoS_2 films exhibit poor electrical properties, with relatively low field effect mobility for a transistor (typically < 15 $cm^2 V^{-1} s^{-1}$),[14–20] compared to pristine MoS_2 bulk monocrystals. Especially, as the grains are of submicrometer size, the presence of a large density of grain boundaries is usually the limiting factor concerning carrier transport in MoS_2 films produced by the above methods. The key challenge therefore involves the achievement of highly crystalline 2D layered semiconductor films over a large-area, with a minimum content of structural defects such as grain boundaries. In such a way, it may be anticipated that the excellent electrical and mechanical properties of their single crystal bulk phase will translate to the resulting films.

In the present work, we report for the first time the fabrication of high-mobility 2D layered transistors (≈121 $cm^2 V^{-1} s^{-1}$) based on large-grain and highly crystalline $MoSe_2$ films grown onto SiO_2 substrates by modified chemical vapor deposition (m-CVD). To obtain high quality $MoSe_2$ films, a sophisticated CVD is developed based on precursor polycrystalline compounds of $MoSe_2$ being directly synthesized on SiO_2 insulator. A single grain was selected to perform cross-sectional high-resolution scanning/transmission electron microscopy (HR-S/TEM) and X-ray diffraction (XRD) analyses, which reveal that the individual grains consist of a well-defined $MoSe_2$ crystal structure (stacking sequence ≈"2H phase"), without noticeable structural defects, and relatively large grain size (>several hundred μm), covering the entire surface of a 2 in. Si wafer. The stoichiometric ratio of Mo:Se obtained from the integrated Mo and Se 3d peak areas of high-resolution X-ray photoelectron spectroscopy (XPS) is ≈2, indicating that the chemical composition indeed consists of $MoSe_2$. A field effect device fabricated onto such an $MoSe_2$ single grain exhibits high-mobility n-type thin-film transistor characteristics which inherit the excellent properties of field-effect mobility up to 121 $cm^2 V^{-1} s^{-1}$, a high self-gain, high on/off current ratio (>10^4) on plastic PI film or a

 © 2016 WILEY-VCH Verlag GmbH & Co. KGaA, Weinheim

rigid Si wafer. Such performance of as-grown CVD films is close to that of a single-crystal $MoSe_2$ bulk. An $MoSe_2$ transistor fabricated on a flexible polyimide substrate preserves its electrical performance even after being subjected to mechanical bending test inward and outward at a radius of curvature as small as 5 mm. The overall results suggest that highly crystalline CVD $MoSe_2$ films are promising candidates for the realization of flexible electronics or high-speed integrated circuits.

The precursor polycrystalline compounds of $MoSe_2$ (p-$MoSe_2$) were synthesized by solid state reaction.[21] Mo powder (–400 mesh, 99.95%) and Se shot (99.999%) were loaded in an evacuated quartz ampoule (under 10^{-5} torr) and heated at 950 °C for 3 d. The single-crystalline platelets of $MoSe_2$ on Si substrate were prepared by modified direct vapor transport method using the vertical three-zone tube furnace.[22] We used the Mo-coated Si substrate (with a Mo thickness of 10 nm) in order to increase the wettability of the $MoSe_2$ layer. The polycrystalline precursor p-$MoSe_2$ compound and Mo-coated Si substrate were located at the bottom and the top side of the evacuated quartz ampoule, respectively. We applied a temperature gradient of 50 °C between the cold side of Mo-coated Si substrate and the hot side of the p-$MoSe_2$ precursor. The precursor p-$MoSe_2$ and Mo-coated Si substrate were slowly heated up to 1050 and 1000 °C, respectively, and kept at the same temperatures for 7 d in an evacuated quartz ampoule using the multizone furnace.

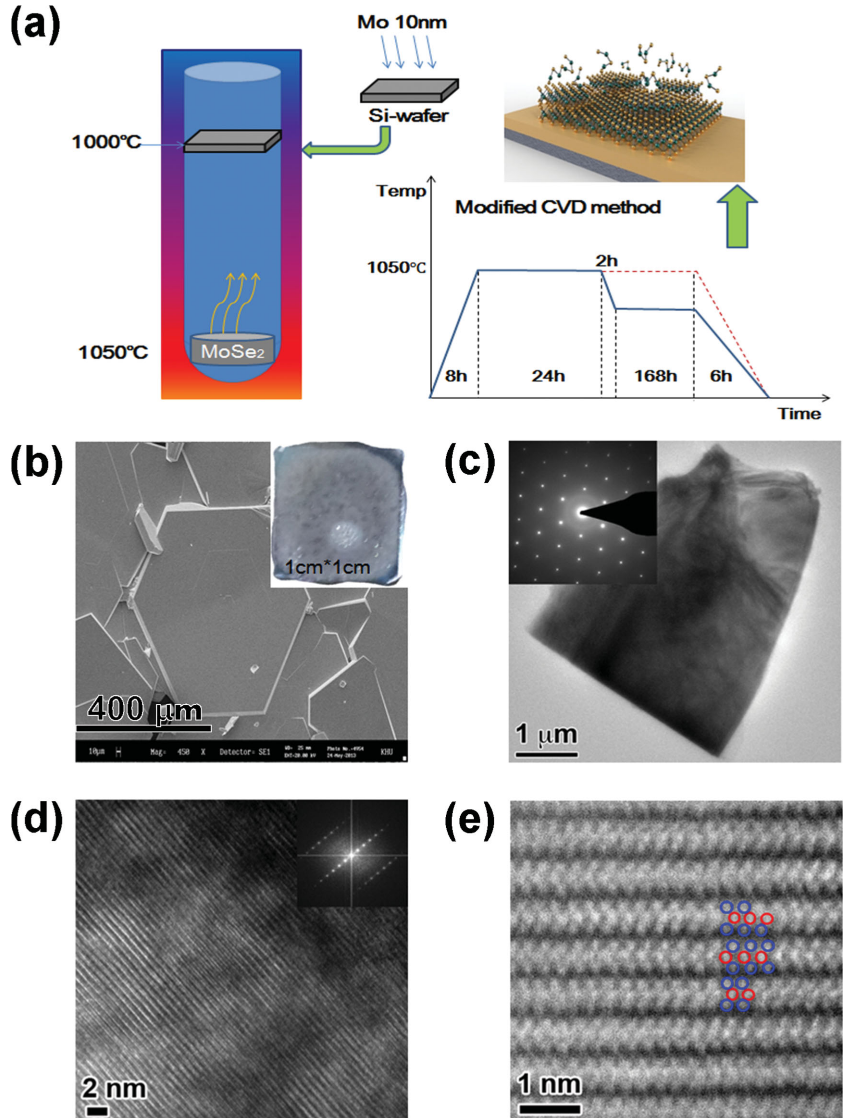

Figure 1. Synthesis and microstructures of $MoSe_2$ film. a) Schematic representation for synthesizing multilayer $MoSe_2$ films. b) SEM image of as-synthesized $MoSe_2$ film. Inset shows a photograph of CVD-grown thin $MoSe_2$ film on Si wafer capped with 300 nm SiO_2. c) Plan-view TEM image of a dispersed $MoSe_2$ particle. The inset shows a selected area electron diffraction (SAED) pattern from within the particle. d) High-resolution TEM image and e) aberration-corrected high angle annular dark field (HAADF) STEM images of cross-sectional $MoSe_2$ film. Inset in (d) is a fast Fourier transform (FFT) from the layered $MoSe_2$ structure in (d).

Figure 1a,b shows a schematic representation of synthesis process of $MoSe_2$ film and an SEM image of an as-synthesized $MoSe_2$ film under optimized conditions, respectively. Compared to single or few layered $MoSe_2$ films with triangular shaped grains, which are synthesized by conventional CVD methods,[23,24] the film mainly consists of hexagonal grains ranging over several micrometers. In single or few layered $MoSe_2$ films, the difference in edge formation energy depending on Mo-edge $\left(10\bar{1}0\right)$ or Se-edge $\left(\bar{1}010\right)$ termination results in triangular shaped grains, but since the effect of specific edge termination is canceled out by alternating Mo- and S-edges in multilayer $MoSe_2$ films, a hexagonal shape is expected from the crystal structure.[25] Figure 1c represents a plan-view TEM image of a dispersed $MoSe_2$ particle, and inset in Figure 1c is a selected area electron diffraction (SAED) pattern taken from within the particle. The size of the particle in Figure 1c is ≈5 μm and the diffraction patterns indicate that the $MoSe_2$ particle consists of a single hexagonal grain observed along the [0002] zone. A high-resolution cross-sectional TEM image of the $MoSe_2$ film is shown in Figure 1d, clearly revealing layered structures. The inset in Figure 1d is a fast Fourier transform (FFT) from the whole image of Figure 1d. This FFT pattern represents the hexagonal 2H structure from the $[2\bar{1}\bar{1}0]$ zone axis. The inset in Figure 1d is an FFT from the corresponding image, reflecting the hexagonal 2H structure along the $[2\bar{1}\bar{1}0]$ zone axis. The unit cell of the hexagonal 2H structure consists of two Se-Mo-Se layers, which exhibit A-B type stacking sequence. In each Se-Mo-Se layer, the top Se layer is trigonal-prismatically coordinated with the bottom Se layer throughout the Mo interlayer. Trigonal prismatic coordination of two Se layers (red circles) through an Mo interlayer (blue circles) is observed in a high-resolution high angle annular dark field (HAADF) STEM image as shown in Figure 1e. The Mo layer in

© 2016 WILEY-VCH Verlag GmbH & Co. KGaA, Weinheim

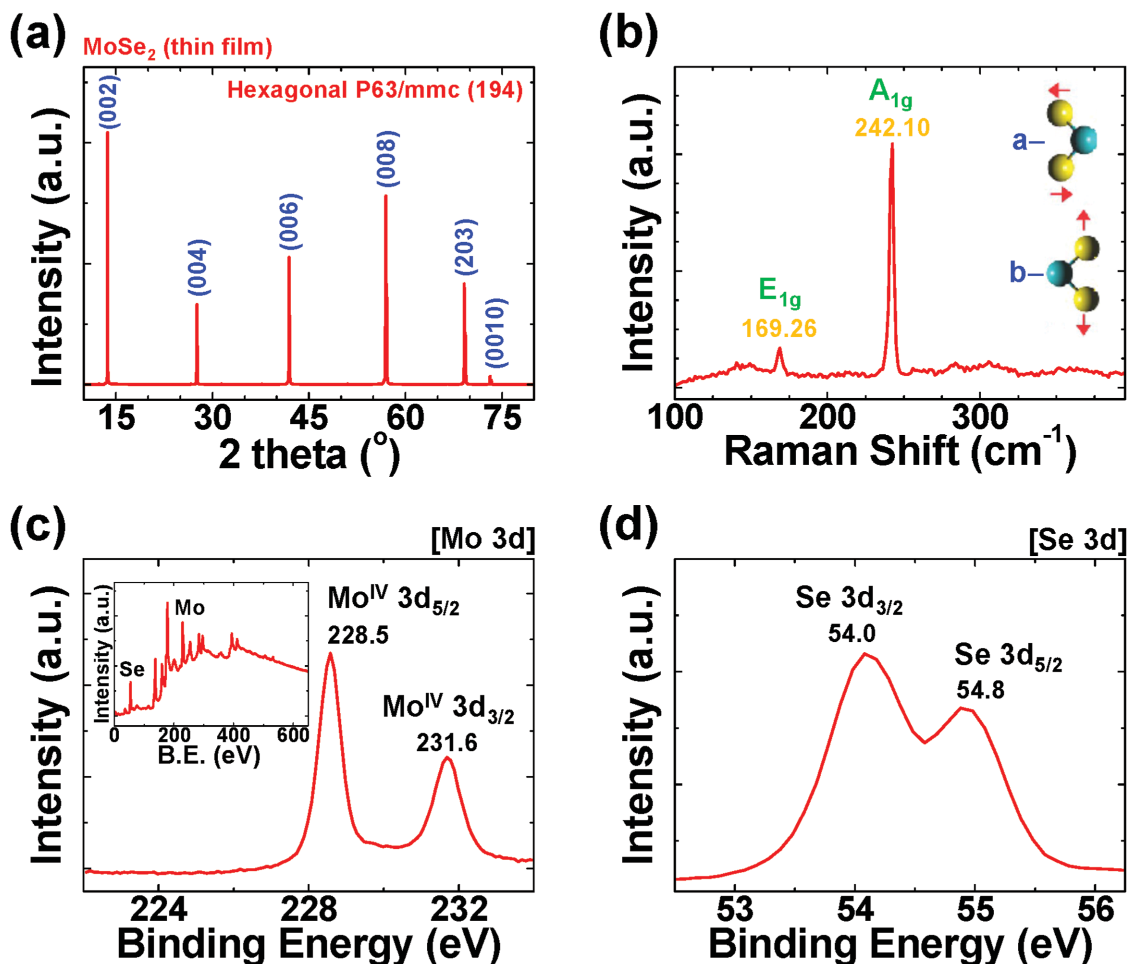

Figure 2. Spectroscopic analyses of the large-area 2D $MoSe_2$ film synthesized by modified chemical vapor transport (m-CVD). a) XRD pattern of a multilayer $MoSe_2$ film (the Si peak is subtracted). b) Raman characterization of a multilayer $MoSe_2$ film with schematic representation of phonon active modes. c,d) XPS peaks of Mo and Se elements in the $MoSe_2$ film. Inset shows the data of whole range of an XPS survey spectrum.

each Se-Mo-Se stack acts as a mirror plane between the top and bottom Se layers. Also, the upper and lower Se-Mo-Se layers with respect to an Se-Mo-Se layer are mirror images of each other, confirming that the synthesized $MoSe_2$ has the 2H hexagonal structure.

To assess the quality of the $MoSe_2$ grown, grazing incidence angle XRD patterns were recorded in order to elucidate the overall crystallinity. **Figure 2**a shows the XRD pattern recorded from $MoSe_2$ films deposited on a silicon substrate. The XRD patterns of the present material match well the characteristic peaks of standard $MoSe_2$ obtained at 2θ values of 13.69°, 27.57°, 41.9°, 56.93°, 69.13°, and 73.13°. The latter confirms that the samples have a hexagonal structure.[26] The XRD peaks correspond to Bragg diffraction of the (002), (004), (006), (008), (203), and (00 10) planes. The strongest peak is found to be located near $2\theta = 13.69°$. This peak corresponds to the (002) plane of the hexagonal crystal structure corresponding to the D^4_{6h} ($P6_3$/mmc-194) space group. The XRD patterns match the literature data of the diffraction peaks of crystalline molybdenum diselenide[27,28] and suggest the as-prepared products indeed consist of $MoSe_2$. The obtained product has a hexagonal lattice with the lattice parameters $a = b = 3.2881$ Å and $c = 12.9162$ Å that are consistent with the JCPDS No. 77-1715 for the referred $MoSe_2$ material.[29] The presence of (00*l*) peaks such as (002), (004), (006), and (008) indicate that the layers are well-oriented along the *c*-axis.

Raman spectroscopy was also utilized to further investigate the crystal structure and thickness of 2D $MoSe_2$ thin films as shown in Figure 2b (λ_{ex} = 514 nm). In each case, a number of well-defined peaks are observed between 100 and 400 cm^{-1}. Such peaks are generally used to identify layered compounds as reported in the literature.[28,30,31] The spectra of Figure 2b acquired with an incident laser power of 50 mW presents two major peaks at (a) 169.26 and (b) 242.10 cm^{-1} corresponding to the E_{1g} and A_{1g} modes, respectively.[32] They are Raman active related modes and the corresponding atomic motions are shown in Figure 2b. For multilayer $MoSe_2$, the A_{1g} mode occurs at a higher frequency with respect to the E_{1g} mode. This observation is consistent with the earlier studies[33,34] in which the A_{1g} mode was better resolved at longer excitation wavelengths. The A_{1g} peak FWHM is 2.46 cm^{-1}, assuming in all cases a Lorentzian fit. The intensity ratio between the A_{1g} and E_{1g} ($I_{A_{1g}}/I_{E_{1g}}$) mode is found to be 6.181. Furthermore, this intensity ratio value between A_{1g} and E_{1g} is lower and represents the multilayer $MoSe_2$ films.

© 2016 WILEY-VCH Verlag GmbH & Co. KGaA, Weinheim

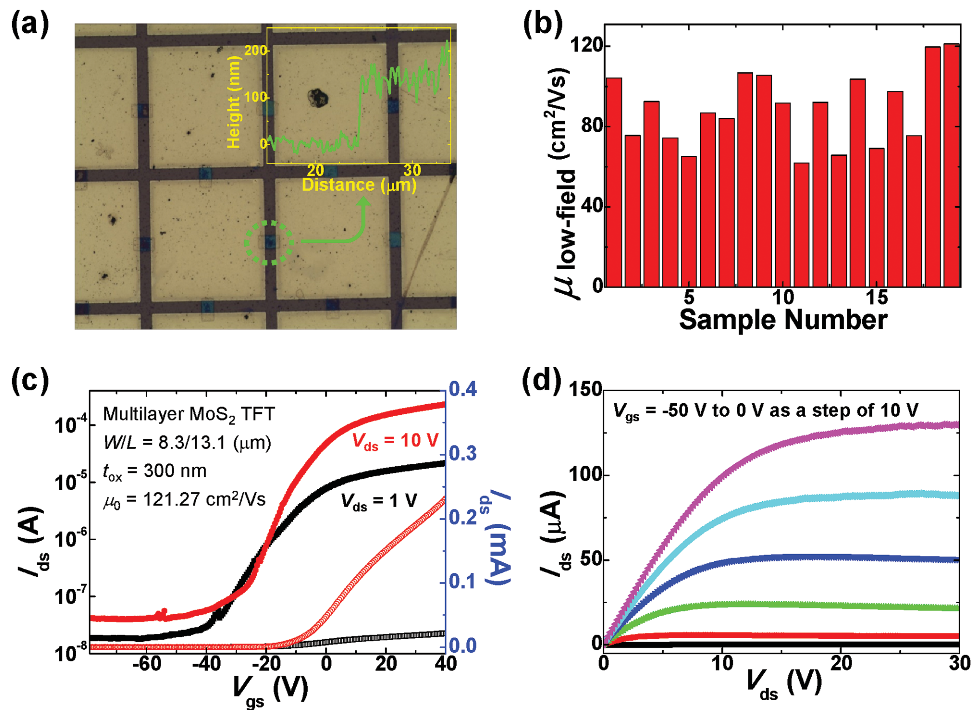

Figure 3. Electrical characteristics of a $MoSe_2$ transistor on a rigid substrate. a) Optical images of fabricated $MoSe_2$ transistors array. Inset shows that the thickness of $MoSe_2$ channels measured by AFM height profile was in the range of 100–150 nm. b) Histogram of a low-field mobility for 19 $MoSe_2$ transistors. c) Transfer characteristics of $MoSe_2$ transistor. The devices show a maximum low-field mobility 121 $cm^2\ V^{-1}\ s^{-1}$. d) Experimental output characteristics with clear saturation behavior up to a drain voltage of 30 V.

The chemical compositions of $MoSe_2$ in the CVD grown films were examined with XPS. As shown in Figure 2c,d, two elements present in the spectra acquired Mo and Se. The wide scanning of the XPS spectra is shown in the inset of Figure 2c. The 3d spectra of Mo and Se in the $MoSe_2$ sample have $Mo3d_{3/2}$, $Mo3d_{5/2}$, $Se3d_{3/2}$, and $Se3d_{5/2}$ peaks which can be observed at 231.6, 228.5, 54.0, and 54.8 eV, respectively. Mo $3d_{5/2}$ and Mo $3d_{3/2}$ core level peaks are located at the binding energy of 228.5 and 231.6 eV confirming that molybdenum is in its Mo(IV) state and suggesting the dominance of the +4 oxidation state; and the 3d peak of Se element is split into well-defined $3d_{5/2}$ and $3d_{3/2}$ peaks at binding energy of 54.8 and 54.0 eV corresponding to the −2 oxidation state of selenium which is in agreement with the values obtained in other $MoSe_2$ systems. The former positions indicate the reduction of Mo from Mo^{6+} to Mo^{4+}: peaks are significantly shifted from their hexavalent positions of 231.6 and 228.5 eV and the peak of Se can be divided around 54 eV. The concentration ratio of Mo:Se is ≈2, suggesting that the CVD grown $MoSe_2$ is reasonably stoichiometric.

Figure 3 shows the measured current–voltage (I–V) characteristics for a highly crystalline $MoSe_2$-TFTs fabricated on a 300 nm thick SiO_2 gate insulator (gate length of 13.1 µm and an overall width of 8.3 µm). The electrical performance of field effect transistors based on large-scale synthetic polycrystalline MoS_2 or $MoSe_2$ to date used to be limited by the presence of small submicrometer grains and their boundaries.[35,36] These grains are small or even microscopic crystal, and their orientation is randomly distributed without preferred direction, which can degrade carrier transport in a transistor—a prime determinant of device performance in CVD grown film. However, spectroscopic analyses in Figures 2 reveal that our well-defined $MoSe_2$ films consist of highly crystalline grains of the same microstructure. Plan-view TEM analyses indicate that a single domain consists of monocrystalline $MoSe_2$. Thus, an active channel fabricated within a large single grain is not affected by structural defects such as grain boundaries, and the corresponding transistor exhibits excellent electrical performance: the low-field mobility (μ_0) as high as 121 $cm^2\ V^{-1}\ s^{-1}$ without the influence of contact resistance (Y function method),[35] on/off current ratios as high as 10^4, and robust current saturation over a high drain voltage window—all with levels of uniformity and reproducibility in unipolar n-type behavior.

In order to fabricate mechanically flexible TFTs, single-crystalline multilayer $MoSe_2$ flakes were transferred onto PI substrates. An organic gate dielectric (e.g., SU-8 2000.5, Microchem) was used in order to enhance the mechanical reliability of the device. The representative $MoSe_2$ TFT with this geometry in **Figure 4**a shows excellent transistor performances without mechanical bending. The mobility (μ_{eff}) values, deduced from a standard model of metal-oxide-semiconductor transistor and a transconductance ($g_m = dI_d/dV_g$) extracted from IV curves, are as high as 120 $cm^2\ V^{-1}\ s^{-1}$ and typically ≈80 $cm^2\ V^{-1}\ s^{-1}$, with an on/off current ratio over 10^4. To investigate the variation of the transistor performances under the mechanical stresses, the $MoSe_2$ TFTs array on PI/PET substrate were bent by using multimodal bending tester (Covotech Co., Ltd), as shown in Figure 4a. The tensile stress due to the upward bending was applied parallel to the $MoSe_2$ channels (inset of Figure 4a).

© 2016 WILEY-VCH Verlag GmbH & Co. KGaA, Weinheim

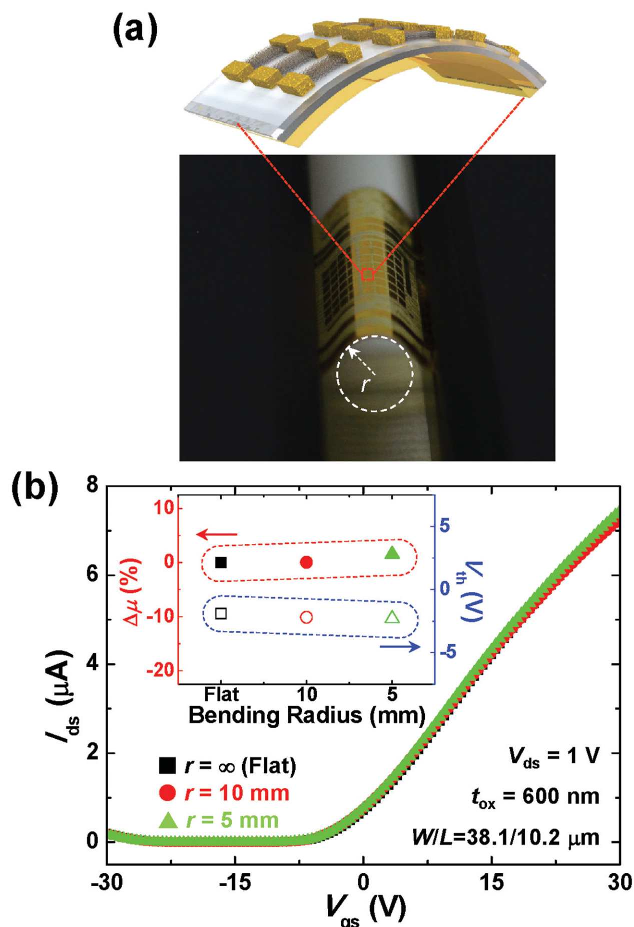

Figure 4. Electrical characteristics of a flexible $MoSe_2$ transistor under mechanical bending test. a) Schematic cross section of a collection of an $MoSe_2$ transistor on a flexible PI/PET substrate (above) and photograph of experimental setup for multimodal bending test with a different radii (below). b) Measured drain current versus gate voltage of an enhancement-mode $MoSe_2$ transistor as a function of bending radius. Black dots denote the *I–V* characteristics in the unbent state. The inset consists of plots of $\Delta\mu$ and V_{th} for a flexible $MoSe_2$ transistor, exhibiting negligible variations under mechanical stress with different bending radii.

The bending radius was controlled through tangential contact of rigid cylinder with pre-defined radius, and electrical properties of a flexible $MoSe_2$ TFT were examined under flat (i.e., not bent) and static bending environments at different radii (r = 10 and 5 mm). When the bending radius (r) is 5 mm, the generated maximum tensile stress in the outermost area (interface between the gate electrode and the PI substrate) is 4.38×10^5 N m^{-2} with a strain of 0.2%.

Figure 4b shows the transfer (I_d–V_g) characteristics of the $MoSe_2$ TFT under flat or bent conditions. The I_d–V_g curves of the $MoSe_2$ TFT at a bending radius of 10 and 5 mm did not change significantly with respect to that measured in flat condition. As shown in the inset of Figure 4b, the mobility variations ($\Delta\mu$ (%) = $|\mu_{bending} - \mu_{flat}|/\mu_{flat}$) due to the bending with r = 10 and 5 mm were 0.05% and 1.53% (solid symbols), respectively. The threshold voltage of the $MoSe_2$ TFT under flat condition was −1.9 V. As bending radius decreased, the threshold voltage was shifted negatively to −2.2 V (r = 10 mm) and −2.3 V (r = 5 mm) (empty symbols). After the measurements are done in bending conditions, the TFT properties recover their initial values as the substrate is flattened again. The $MoSe_2$ TFTs therefore have a solid tolerance against mechanical stress.

In conclusion, the uniform growth of large grain multilayer $MoSe_2$ films on insulator substrates was demonstrated using a modified chemical vapor deposition method. Highly crystalline $MoSe_2$ film with large grain sizes was fabricated as an active channel for a transistor, consisting of bottom gate architecture with Ti/Au source and drain, on flexible plastic substrate or a rigid Si wafer. Our multilayer $MoSe_2$ field-effect transistors exhibited high mobility (≈121 cm^2 V^{-1} s^{-1}), a high on/off current ratio (>10^4), and good mechanical flexibility while bending down to radii of 5 mm. The experimental results can be understood remarkably well by classical long-channel MOSFET theory. The $MoSe_2$ films presented in this work are attractive for the fabrication of high speed thin-film devices for flexible integrated circuits, especially for applications such as humanoid robotics, flexible OLED displays, and human-centric soft electronics.

Experimental Section

Flexible $MoSe_2$ Transistor on Flexible PI Substrate: The bottom Ti (20 nm)/Al (50 nm) gate electrodes were deposited by electron beam evaporation on flexible PI substrate. After forming the gate electrode, an organic dielectric material (Su-8 2000.5, Microchem) was spin-coated to reach a thickness of 650 nm, followed by baking on a hot plate. The $MoSe_2$ film was transferred using sequential steps to the surface of the substrate. After depositing Ti/Au (20 nm/100 nm) layer through e-beam evaporator, source–drain electrodes were patterned by conventional photolithography and etching.

Materials Characterization (versus Spectroscopic Analysis): The as-prepared material was characterized by XRD, SEM, TEM, Raman spectroscopy, and XPS. Crystal faces were identified and scanned by using an HP thin film X-ray diffractometer (D8 Advance, Bruker Corporation) Ni filtered with Cu-Kα irradiation (40 kV, 100 mA, λ = 0.15405 nm) and a sol-X energy-dispersive detector with the angular range of 2θ from 10° to 80° with a step size of 0.04° and a collection time of 3–4 s. Morphologies were characterized using scanning electron microscope (HITACHI-S 4800). SEM was performed with a 15 kV acceleration voltage in the top view by detecting the secondary electron emission from the sample. The S/TEM images were observed using a C_S-corrected scanning/transmission electron microscope (JEOL: JEM-ARM 200F) and conventional transmission electron microscope (FEI Tecnai F20), both of which were operated at an acceleration voltage of 200 kV. The Raman spectra were obtained using HR Raman spectrometer (Invid Raman microscope, Renishaw) and laser with wavelength 514 nm. The information of binding energies in $MoSe_2$ was characterized by using an X-ray photoelectron spectrometer (Thermo:Electron). XPS measurements were performed with a Kα X-ray source on the samples to verify the presence of Mo and Se.

Acknowledgements

This research was supported by the National Research Foundation of Korea (NRF-2013M3C1A3059590 and NRF-2014M3A9D7070732), the Industrial Strategic Technology Development Program (10045145), and through the NCN-NEEDs program, which was funded by the National Science Foundation (Contract No. 1227020-ECE) and by the Semiconductor Research Corporation. This work was partially supported

© 2016 WILEY-VCH Verlag GmbH & Co. KGaA, Weinheim

by the Korea Institute of Science and Technology (KIST) Institutional Program (Project No. 2Z04470).

Note: The presentation of the author name Won Geun Song was corrected on March 17, 2016, after initial publication online.

Received: September 29, 2015
Revised: November 16, 2015
Published online: January 11, 2016

[1] S. Kim, H.-J. Kwon, S. Lee, H. Shim, Y. Chun, W. Choi, J. Kwack, D. Han, M. Song, S. Kim, S. Mohammadi, I. Kee, S. Y. Lee, *Adv. Mater.* **2011**, *23*, 3511.
[2] D.-H. Kim, N. Lu, R. Ma, Y.-S. Kim, R.-H. Kim, S. Wang, J. Wu, S. M. Won, H. Tao, A. Islam, K. J. Yu, T.-I. Kim, R. Chowdhury, M. Ying, L. Xu, M. Li, H.-J. Chung, H. Keum, M. McCormick, P. Liu, Y.-W. Zhang, F. G. Omenetto, Y. Huang, T. Coleman, J. A. Rogers, *Science* **2011**, *333*, 838.
[3] L. Gao, Y. Zhang, V. Malyarchuk, L. Jia, K.-I. Jang, R. C. Webb, H. Fu, Y. Shi, G. Zhou, L. Shi, D. Shah, X. Huang, B. Xu, C. Yu, Y. Huang, J. A. Rogers, *Nat. Commun.* **2014**, *5*, 4938.
[4] D.-H. Kim, R. Ghaffari, N. Lu, J. A. Rogers, *Annu. Rev. Biomed. Eng.* **2012**, *14*, 113.
[5] S. Y. Lee, K.-I. Park, C. Huh, M. Koo, H. G. Yoo, S. Kim, C. S. Ah, G. Y. Sung, K. J. Lee, *Nano Energy* **2012**, *1*, 145.
[6] S. C. B. Mannsfeld, B. C.-K. Tee, R. M. Stoltenberg, C. V. H.-H. Chen, S. Barman, B. V. O. Muir, A. N. Sokolov, C. Reese, Z. Bao, *Nat. Mater.* **2010**, *9*, 859.
[7] G. Schwartz, B. C.-K. Tee, J. Mei, A. L. Appleton, D. H. Kim, H. Wang, Z. Bao, *Nat. Commun.* **2013**, *4*, 1859.
[8] S. Kim, A. Konar, W.-S. Hwang, J. H. Lee, J. Lee, J. Yang, C. Jung, H. Kim, J.-B. Yoo, J.-Y. Choi, Y. W. Jin, S. Y. Lee, D. Jena, W. Choi, K. Kim, *Nat. Commun.* **2012**, *3*, 1011.
[9] W. Choi, M. Y. Cho, A. Konar, J. H. Lee, G.-B. Cha, S. C. Hong, S. Kim, J. Kim, D. Jena, J. Joo, S. Kim, *Adv. Mater.* **2012**, *24*, 5832.
[10] B. Radisavljevic, A. Radenovic, J. Brivio, V. Giacometti, A. Kis, *Nat. Nanotechnol.* **2011**, *6*, 147.
[11] H.-J. Kwon, W. Choi, D. Lee, Y. Lee, J. Kwon, B. Yoo, C. P. Grigoropoulos, S. Kim, *Nano Res.* **2014**, *7*, 1137.
[12] S. Wu, J. S. Ross, G.-B. Liu, G. Aivazian, A. Jones, Z. Fei, W. Zhu, D. Xiao, W. Yao, D. Cobden, X. Xu, *Nat. Phys.* **2013**, *9*, 149.
[13] K. He, C. Poole, K. F. Mak, J. Shan, *Nano Lett.* **2013**, *13*, 2931.
[14] T. B. Baker, R. M. McFall, V. Shoham, *Psychol. Sci. Public Interest* **2009**, *9*, 67.
[15] J. Wilson, *Surf. Sci.* **1975**, *53*, 330.
[16] Y.-H. Lee, X.-Q. Zhang, W. Zhang, M.-T. Chang, C.-T. Lin, K.-D. Chang, Y.-C. Yu, J. T.-W. Wang, C.-S. Chang, L.-J. Li, T.-W. Lin, *Adv. Mater.* **2012**, *24*, 2320.
[17] Y. Zhan, Z. Liu, S. Najmaei, P. M. Ajayan, J. Lou, *Small* **2012**, *8*, 966.
[18] A. M. van der Zande, P. Y. Huang, D. A. Chenet, T. C. Berkelbach, Y. You, G.-H. Lee, T. F. Heinz, D. R. Reichman, D. A. Muller, J. C. Hone, *Nat. Mater.* **2013**, *12*, 554.
[19] K.-K. Liu, W. Zhang, Y.-H. Lee, Y.-C. Lin, M.-T. Chang, C.-Y. Su, C.-S. Chang, H. Li, Y. Shi, H. Zhang, C.-S. Lai, L.-J. Li, *Nano Lett.* **2012**, *12*, 1538.
[20] C. Jeong, P. Nair, M. Khan, M. Lundstrom, M. A. Alam, *Nano Lett.* **2011**, *11*, 5020.
[21] E. Revolinsky, D. Beerntsen, *J. Appl. Phys.* **1964**, *35*, 2086.
[22] C. Sumesh, K. Patel, V. Pathak, R. Srivastav, *Cryst. Res. Technol.* **2010**, *45*, 957.
[23] X. Wang, Y. Gong, G. Shi, W. L. Chow, K. Keyshar, G. Ye, R. Vajtai, J. Lou, Z. Liu, E. Ringe, B. K. Tay, P. M. Ajayan, *ACS Nano* **2014**, *8*, 5125.
[24] J. C. Shaw, H. Zhou, Y. Chen, N. O. Weiss, Y. Liu, Y. Huang, X. Duan, *Nano Res.* **2014**, *7*, 1.
[25] S. Helveg, J. V. Lauritsen, E. Laegsgaard, I. Stensgaard, J. K. Norskov, B. S. Clausen, H. Topsoe, F. Besenbacher, *Phys. Rev. Lett.* **2000**, *84*, 951.
[26] J. Fuhr, J. Sofo, A. Saúl, *Phys. Rev. B* **1999**, *60*, 8343.
[27] R. Bissessur, H. Xu, *Mater. Chem. Phys.* **2009**, *117*, 335.
[28] S. Larentis, B. Fallahazad, E. Tutuc, *Appl. Phys. Lett.* **2012**, *101*, 223104.
[29] T. N. Blanton, T. C. Huang, H. Toraya, C. R. Hubbard, S. B. Robie, D. Louer, H. E. Gobel, G. Will, R. Gilles, T. Raftery, *Powder Diffr.* **1995**, *10*, 91.
[30] P. Tonndorf, R. Schmidt, P. Bottger, X. Zhang, J. Borner, A. Liebig, M. Albrecht, C. Kloc, O. Gordan, D. R. T. Zahn, S. M. de Vasconcellos, R. Bratschitsch, *Opt. Express* **2013**, *21*, 4908.
[31] S. Tongay, J. Zhou, C. Ataca, K. Lo, T. S. Matthews, J. Li, J. C. Grossman, J. Wu, *Nano Lett.* **2012**, *12*, 5576.
[32] S. Sugai, T. Ueda, *Phys. Rev. B* **1982**, *26*, 6554.
[33] C. Lee, H. Yan, L. E. Brus, T. F. Heinz, J. Hone, S. Ryu, *ACS Nano* **2010**, *4*, 2695.
[34] Y. Zhang, T.-R. Chang, B. Zhou, Y.-T. Cui, H. Yan, Z. Liu, F. Schmitt, J. Lee, R. Moore, Y. Chen, H. Lin, H.-T. Jeng, S.-K. Mo, Z. Hussain, A. Bansil, Z.-X. Shen, *Nat. Nanotechnol.* **2013**, *9*, 111.
[35] G. Ghibaudo, *Electron. Lett.* **1988**, *24*, 543.
[36] A. W. Tsen, L. Brown, M. P. Levendorf, F. Ghahari, P. Y. Huang, R. W. Havener, C. S. Ruiz-Vargas, D. A. Muller, P. Kim, J. Park, *Science* **2012**, *336*, 1143.

© 2016 WILEY-VCH Verlag GmbH & Co. KGaA, Weinheim